Journal of Electroanalytical Chemistry 947 (2023) 117785

Contents lists available at ScienceDirect

Journal of Electroanalytical Chemistry

journal homepage: www.elsevier.com/locate/jelechem

$Zn_xCo_{(1-x)}$ coatings from choline chloride-ethylene glycol deep eutectic solvent as electrocatalysts for hydrogen evolution reaction

Deomar N. Rodrigues-Júnior [a], Natalia G. Sousa [a], F. Murilo T. Luna [b], Thiago M.B.F. Oliveira [c], Dieric S. Abreu [d], Walther Schwarzacher [e], Pedro de Lima-Neto [a], Adriana N. Correia [a,*]

[a] Grupo de Eletroquímica e Corrosão, Departamento de Química Analítica e Físico-Química, Centro de Ciências, Universidade Federal do Ceará, Campus do Pici, Fortaleza, CE 60440-900, Brazil
[b] Grupo de Pesquisa em Separações por Adsorção, Departamento de Engenharia Química, Centro de Tecnologia, Universidade Federal do Ceará, Campus do Pici, Fortaleza, CE 60455-760, Brazil
[c] Laboratório de Química Aplicada, Centro de Ciência e Tecnologia, Universidade Federal do Cariri, Juazeiro do Norte, CE 63048-080, Brazil
[d] Laboratório de Materiais e Dispositivos, Departamento de Química Analítica e Físico-Química, Centro de Ciências, Universidade Federal do Ceará, Campus do Pici, Fortaleza, CE 60440-900, Brazil
[e] H. H. Wills Physics Laboratory, University of Bristol, Tyndall Avenue, Bristol, BS8 1TL, United Kingdom

ARTICLE INFO

Keywords:
Water splitting
Hydrogen production
Metallic coatings
Deep eutectic solvents
Electrocatalysis

ABSTRACT

Hydrogen has emerged as a clean and renewable energy and its production by water splitting is a promising production route. However, to meet the demand on a commercial scale, research focusing on more efficient electrocatalysts is necessary. In this work, new findings on Zn, Co and Zn-Co coatings produced in deep eutectic solvent based on choline chloride (ChCl) and ethylene glycol (EG) are reported. Varying the concentrations of Zn^{2+} and Co^{2+} ions in 1ChCl:2EG, crystalline electrodeposits with fine control of composition and morphology were obtained, and which present different reactivity to electrocatalyze the hydrogen evolution reaction (HER) in alkaline medium. The performance of metallic coatings is influenced by temperature, due to changes in viscosity, ionic diffusion coefficient and charge transport in the electrolyte. The results also revealed that increasing the Co content in the coatings, changes occur in the morphological organization, stability, and electrode area, which positively influence the hydrogen production. Among the different coatings tested (Zn, Co, Zn_{96}-Co_4 and Zn_3-Co_{97}), Zn_3-Co_{97} was the most promising in terms of Tafel coefficient (108 mV dec^{-1}), exchange current density (8.57×10^{-6} A cm^{-2}) and overpotential estimated for HER (333 mV at 10 mA cm^{-2}) in 1 mol L^{-1} KOH at 298.15 K, although the other materials also showed electrochemical advantages over the unmodified Cu substrate. The reported data also reiterate the great electrochemical potential of metallic coatings for water splitting and complement the growing energy demand for hydrogen gas.

1. Introduction

The deleterious effects caused to the environment from non-renewable energy sources, such as fossil fuels, coal, and petroleum, require urgent and more sustainable alternatives to reduce greenhouse gas emissions and, consequently, the disastrous effects of global warming [1]. Today, hydrogen stands out among the most promising alternatives, since it can be produced from renewable sources and has a highly attractive energy density per mass (≈ 140 MJ kg^{-1}) and volume (≈ 0.011 MJ kg^{-1}) at room temperature, compared to more traditional fuels [1–4]. One of the great challenges is that there is not freely available and ready-to-use hydrogen, requiring appropriate methods and systems to extract it from energetically stable precursors, such as water and hydrocarbons. Water splitting is simpler and easier to accomplish, and the type of electrocatalyst employed has a significant impact on the HER yield in terms of reaction overpotential, corrosion resistance and resulting current density [1,2,5–7].

It is known that noble metal (Pt, Ru and Ir)-based electrocatalysts are highly reactive toward HER, but their scarcity and high cost make them uneconomic for large-scale production and application [8–13]. Cobalt and its alloys have a better cost-benefit ratio, besides combine different electrochemical advantages (e.g., excellent electrical conductivity, high activity, and stability in alkaline medium) that arouse speculation regarding their efficiency in producing hydrogen by water splitting

* Corresponding author.
E-mail address: adriana@ufc.br (A.N. Correia).

https://doi.org/10.1016/j.jelechem.2023.117785
Received 25 July 2023; Received in revised form 29 August 2023; Accepted 7 September 2023
Available online 14 September 2023

[14–17]. Such performance is linked to several parameters of synthesis and application of these materials, which must be meticulously studied and continuously improved. Fan et al. [18] studied cobalt-coated copper substrates as HER electrocatalysts in 30 wt% KOH. These authors identified remarkable changes in the structural arrangement, morphology, and reactivity of the electrodeposits according to the electrolytic medium, presence of oxygen and temperature of synthesis, so that the lowest overpotential and highest surface roughness factor for HER was obtained from an acetate-enriched solution, kept at 25 °C. Maurya et al. [19] also showed reactivity changes when HER was promoted in 1 mol/L KOH, using Ni-Co coatings immobilized onto copper and steel derived substrates as electroactive surfaces, suggesting a synergistic effect of intercalated materials in the electrode configuration. Kublanovsky and Yapontseva [20] found that electrodeposited Co-Mo alloys can have better electrocatalytic properties in alkaline medium (reduction in HER overpotential around 400 mV) than pure Co, especially when obtained from 10:1% (v/v) Co:Mo compositions. Ling et al. [21] also reported that doping CoO nanorods with Ni and Zn has an important electrocatalytic effect for HER in alkaline medium, Zn being responsible for modulating bulk electronic structure and boost electrical conduction. Other Zn-containing materials have been successfully applied as electrocatalysts for water splitting. Sumesh [22] prepared zinc oxide functionalized molybdenum disulfide heterostructures (MoS_2·ZnO) and tested them for HER electrocatalysis in acidic medium, without compromising their structural stability. Additionally, Cao et al. [23] worked with metal-dopped carbon nanotubes and found that Zn both reduced charge-transfer resistance and increased the proportion of reactive sites available to produce hydrogen.

Since Co and Zn have a positive effect on water splitting, coatings made with combinations of them can achieve superior performance and deserve more attention. Electrodeposition is a simple and low-cost way to produce Zn-Co electrocatalysts for HER, either by potentiostatic or galvanostatic mode [24]. However, the electrosynthesis of metallic coatings from aqueous solutions can compromise their stability due to the existence of parallel reduction reactions, including HER itself. There are also limitations regarding cathodic efficiency, working potential range, and electrodeposit adhesion. Water volatility also narrows the working temperature range, leading to frequent need for electrolyte bath additives and increased laboratory waste [25,26].

Deep eutectic solvents (DES) overcome the limitations and provide a wide range of working potential for electrodepositing various metals and alloys. They are non-ideal liquid mixtures of organic salts with hydrogen bond donors, such as amides, amines, alcohols and carboxylic acids. DES still have high electrical conductivity and solubility for metallic salts, are non-flammable even at relatively high temperatures, biodegradable, produced simply and cheaply [25,27–29]. In the electrodeposition of metals and alloys, DES formed by choline chloride (ChCl) and ethylene glycol (EG) have been used with great success [30–33]. From this perspective, the main objective of this work was to produce coatings of Zn, Co, and Zn-Co from ChCl/EG-based DES, as well as to evaluate the physicochemical properties and effectiveness of these electrodeposits to promote HER in alkaline environment.

2. Experimental procedures

2.1. Chemicals and electrolytic solutions

ChCl, EG, zinc chloride ($ZnCl_2$) and cobalt chloride ($CoCl_2$) were purchased from Sigma-Aldrich and used as received. ChCl and EG were mixed in a 1:2 M ration (1ChCl:2EG) and heated to 353 K until a colorless and homogeneous liquid was formed [15]. The electrodeposition solutions were obtained by dissolving $ZnCl_2$ (0.025 mol/L or 0.4 mol/L Zn^{2+}) and $CoCl_2$ (0.025 mol/L or 0.4 mol/L Co^{2+}) in 1ChCl:2EG, under constant agitation. Since the electric conductivity of the electrolytes strongly depends on the water content, this parameter was determined by Karl Fischer coulometric titration (899 coulometer, Metrohm) in freshly prepared DES mixtures. The water content in 1ChCl:2EG was 13.25 ± 0.06 ppm and ranged from 23.32 ± 0.13 to 57.87 ± 0.31 ppm after adding Zn^{2+} and Co^{2+}.

2.2. Electrochemical experiments

Electrochemical experiments were carried out using a glass electrochemical cell configured with three electrodes. The working electrode was a copper disc embedded in epoxy resin, with an exposed geometric area of approximately 0.023 cm^2. Before each experiment, the working electrode was mechanically polished with 100, 400 and 600-grain size sandpaper, following this sequence, and washed with Milli-Q® water (18.2 MΩ cm). A platinum plate (1 cm^2 geometric area; 99.5% purity) and a silver wire covered with AgCl and immersed in 1ChCl:2EG, were used as auxiliary and reference electrodes, respectively. The tests were carried out in a potentiostat/galvanostat AUTOLAB PGSTAT30, Metrohm-Eco Chemie, controlled by NOVA 2.1 software.

Electrodeposition processes of metallic coatings were monitored by cyclic voltammetry (CV) at 5 mV s^{-1}, keeping the system at 343 K. The ion diffusion coefficients in the deep eutectic solvent were evaluated at different temperatures (303–343 K), using chronoamperometry data adapted to the Cottrell Equation. For these experiments, three electrochemical potentials (i.e., −0.4, −0.8 and −1.3 V) were evaluated for 60 s, chosen from cyclic voltammetry data registered with a Cu substrate (0.023 cm^2 geometric area) immersed in 1ChCl:2EG containing 0.4 mol/L $CoCl_2$ and 0.4 mol/L $ZnCl_2$.

The influence of metallic coatings and selected experimental conditions on HER were studied by linear sweep voltammetry (LSV) at 0.5 mV s^{-1}, using 1 mol/L KOH at 298 K as electrolyte and $Hg_{(s)}|HgO_{(s)}|OH^-_{(aq)}$ (1 mol/L KOH) as reference electrode [30]. The measured potentials ($E_{Hg/HgO}$) were converted to those of the reversible hydrogen electrode (E_{RHE}), through the following equation:

$$E_{RHE}\,(\mathrm{V}) = E_{Hg/HgO}\,(\mathrm{V}) + 0.095 + 0.059pH \quad (1)$$

Coating stability tests were performed over 100 h in a two-electrode cell, applying an average operating potential of −1.8 V at 10 mA cm^{-2}, being repeated three times. Coatings with a nominal thickness around 1.0 μm were immobilized on copper substrates (0.20 cm^2 geometric area), and the results were compared to those obtained with the same electrode without coating and with an AISI 304 stainless steel electrode (0.18 cm^2 geometric area). The electrical circuit was concluded with a stainless steel AISI 304 counter-electrode (0.69 cm^2 geometric area), immersed together with the working electrode in 1 mol/L KOH at 333 K. The current density was set at 10 mA cm^{-2}, taking into account the high HER yield and stability of the coatings, using a direct current power source monitored by a multimeter at fixed time intervals. Specific mass and viscosity measurements were performed with an Anton Paar's Stabinger viscometer, model SVM 3000.

2.3. Electrodeposition of metallic coatings

Zn and Co electrodeposits were obtained from 1ChCl:2EG electrolytes containing 0.4 mol/L Zn^{2+} and 0.4 mol/L Co^{2+}, without mechanical convection influence. Zn_x-$Co_{(1-x)}$ coatings were obtained from solutions with different Zn^{2+}:Co^{2+} molar ratios, i.e., $[Zn^{2+}] = 0.4$ mol/L and $[Co^{2+}] = 0.025$ mol/L or $[Zn^{2+}] = 0.025$ mol/L and $[Co^{2+}] = 0.4$ mol/L. Electrodeposits were obtained potentiostatically at −1.3 V and 343 K, with charge control to obtain coatings with a nominal thickness of 1 μm.

2.4. Complementary physicochemical characterizations

The surface morphology of the coatings was evaluated using a field emission scanning electron microscope (SEM; FEG-SEM FEI-Quanta 450), operating at 20 keV. The atomic percentages of Zn and Co in the

coatings were determined by energy-dispersive X-ray spectroscopy (EDS), using a spectrometer coupled to the microscope. The crystallinity and composition of electrodeposits were also evaluated by X-ray diffraction (XRD) analyses, using a Rigaku DMAXB diffractometer, which operated with a 2 kW X-ray generator and CuKα copper radiation (λ = 0.154 nm). Crystalline phases were identified using the X-Pert HighScore Plus version 3.0.5 (PANalytical®) program, associating the results with the International Centre for Diffraction Data (ICDD)/Joint Committee on Powder Diffraction Standards (JCPDS) database.

3. Results and discussion

3.1. Electrochemical characterization

Initially, CV studies were performed with cooper substrates at 5 mV s^{-1} in pure ChCl/EG-based DES and after adding Zn^{2+} and Co^{2+}, to monitor and evaluate the efficiency of the electrodeposition conditions employed. The result illustrated in Fig. 1a demonstrated that no process was observed in 1ChCl:2EG, varying the potential between −0.4 V and −1.3 V. Above this range, there was a sharp increase in the current density, due to the decomposition of the eutectic solvent caused by the reduction of hydroxyl groups present in ethylene glycol and choline ions [32]. In Fig. 1b, during the positive scan, three well-defined anodic processes with different intensities appeared between −1.1 and −0.6 V, related to the dissolution of zinc electrodeposits and possible Zn-Cu intermetallic entities. A similar profile was observed by Alesary et al. [34], using a Pt electrode polarized anodically in 1ChCl:2EG containing 0.4 mol L^{-1} Zn^{2+}, keeping the system at 353 K. There is also a crossover of cathodic and anodic currents around −1.1 V, which indicates self-organization of crystals by nucleation and electrodeposit growth.

In Fig. 1c, there is a small increase in cathodic current attributed to cobalt reduction around −0.9 V. Then, a significant increase in the cathodic current at −1.2 V begins, followed by a discrete current loop, resulting from the nucleation of zinc on cobalt. In the anodic scan, there are three well-defined processes related to the dissolution of metals, so that the first two refer to zinc and the last to cobalt. Chu et al. [35] obtained analogous results for Zn-Co coatings, produced from 1ChCl:2U at 353 K, using cyclic voltammetry at 50 mV s^{-1}. They attributed the first two anodic processes (at less positive potentials) to zinc dissolution from different phases of the Zn-Co alloy, followed by dissolution of the cobalt electrodeposits as a third process. In Fig. 1d, there is only one process in the cathodic scan before solvent decomposition. This process results from the reduction of cobalt, as its concentration is 16 times higher than zinc. No process is observed in the anodic scan between −0.4 V and −1.3 V. The observed result is also very similar to that shown in Fig. 1e, whose voltammogram was recorded in the electrochemical cell containing only cobalt.

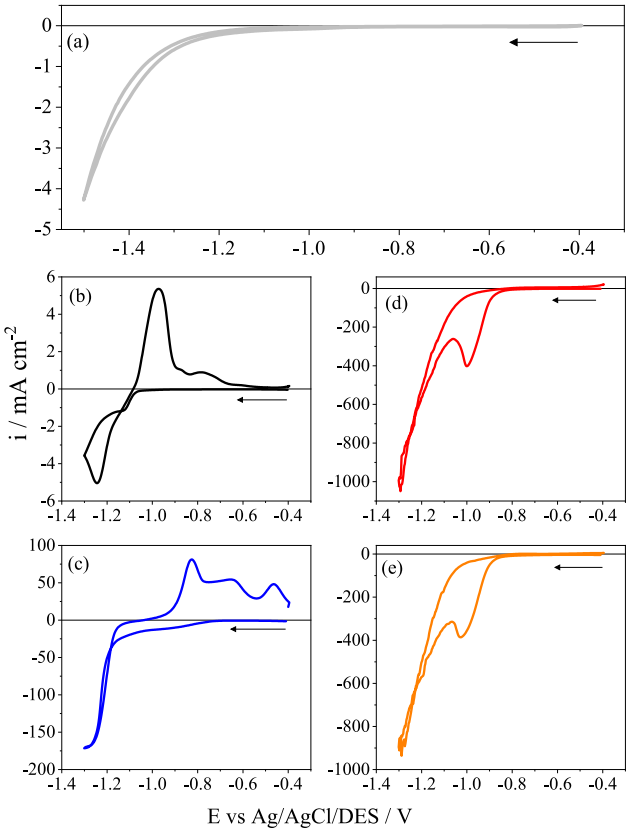

Fig. 1. Cyclic voltammograms obtained at 5 mV s^{-1} in (a) 1ChCl:EG and after adding (b) 0.4 mol L^{-1} $ZnCl_2$, (c) 0.4 mol L^{-1} $ZnCl_2$ + 0.025 mol L^{-1} $CoCl_2$, (d) 0.025 mol L^{-1} $ZnCl_2$ + 0.4 mol L^{-1} $CoCl_2$, (e) 0.4 mol L^{-1} $CoCl_2$.

3.2. Relationship between coating stability, ionic diffusion, and temperature

Chronoamperometric experiments are very useful to examine the electrochemical activity and stability of metallic coatings, especially under temperature gradients. In this work, studying HER at −1.3 V in 1 mol/L KOH (previously optimized condition based on reaction yield and corrosion resistance), an increase in mass-transport-limited current densities was noticed as the temperature increased from 303 K to 343 K, both for Zn and Co-based coatings. This is related to the decrease in the viscosity of the solutions at higher temperatures, which allows faster ion diffusion and a consequent increase in current density. Issues related to mass- and charge-transport variations resulting from temperature changes and their influence on viscosity have also been reported by Fu et al. [36], based on studies on the electrochemical nucleation of copper in ChCl:EG. From the Cottrell Equation [37], it is also possible to verify the impact of the temperature increase on the ionic diffusion coefficient (*D*), as shown in Table 1. For cobalt coatings, *D* values varied between $2.6 \times 10^{-7} \pm 0.7 \times 10^{-8}$ cm^2 s^{-1} and $4.4 \times 10^{-7} \pm 0.5 \times 10^{-7}$ cm^2 s^{-1}, while for zinc coatings the variation was from $8.9 \times 10^{-11} \pm 0.8 \times 10^{-11}$ cm^2 s^{-1} to $4.5 \times 10^{-10} \pm 0.3 \times 10^{-10}$ cm^2 s^{-1}. The same trend was observed by Phuong et al. [38] for the nucleation of Co^{2+} ions in 1ChCl:2U, as the temperature increased from 313 K to 343 K.

For comparison purposes, Table 1 also gathers other *D* values obtained for Co- and Zn-based coatings obtained in different solvents and temperatures [38–44]. For both cases, the values were equivalent to those obtained by other authors who studied coatings produced from the same deep eutectic solvent (7.1×10^{-10} cm^2 s^{-1} at 313 K for Zn^{2+} [43]) or from other compositions, such as ChCl:urea (8.1×10^{-8}–1.1×10^{-7} cm^2 s^{-1} at 313–343 K for Co^{2+} [38]; 7.8×10^{-9} cm^2 s^{-1} at 363 K for Zn^{2+} [41]), EG (2.3×10^{-8} cm^2 s^{-1} at 343 K for Co^{2+} [39]), 1-methyl-imidazolium trifluoromethylsulfonate (7.7×10^{-9} cm^2 s^{-1} at 373 K for Zn^{2+} [40]), urea:1-ethyl-3-methylimidazolium (5.5×10^{-9} cm^2 s^{-1} at 353 K for Zn^{2+} [42]), and hybrid eutectic sulfolane:water (5.0×10^{-12} cm^2 s^{-1} for Zn^{2+} [44]). However, *D* values for Co^{2+} ions in 1ChCl:2EG were higher than those for Zn^{2+} ions recorded under the same experimental conditions. This is due to the formation of a smaller solvation sphere for Co^{2+} ions, giving them greater mobility than Zn^{2+} ions [31,45]. Regardless of the precursor, all coatings remained electrochemically stable at the different HER potentials evaluated, i.e., −0.4, −0.8 and −1.3 V.

3.3. Composition and morphology studies

Fig. 2 presents the percentage elemental composition of electrodeposits obtained by EDS, as well as surface morphological features observed by SEM micrographs, before and after immobilizing the coatings. According to Fig. 2a, the proportion of Zn and Co atoms present in the electrodeposits is very close to their molar concentration contained

Table 1
Comparison of diffusion coefficients obtained for Co^{2+} and Zn^{2+} ions at different temperatures and electrolytes.

Temperature/ K	Electrolyte	D/ $cm^2\ s^{-1}$	Reference
Co^{2+}			
303	1ChCl:2EG	$2.6 \times 10^{-7} \pm 0.7 \times 10^{-8}$	This work
313	1ChCl:2EG	$3.0 \times 10^{-7} \pm 0.8 \times 10^{-8}$	This work
323	1ChCl:2EG	$3.4 \times 10^{-7} \pm 0.5 \times 10^{-7}$	This work
343	1ChCl:2EG	$4.4 \times 10^{-7} \pm 0.5 \times 10^{-7}$	This work
313	1ChCl:2U	8.1×10^{-8}	[32]
323	1ChCl:2U	1.1×10^{-7}	[32]
333	1ChCl:2U	1.1×10^{-7}	[32]
343	1ChCl:2U	1.5×10^{-7}	[32]
343	Ethylene glycol	2.3×10^{-8}	[33]
Zn^{2+}			
303	1ChCl:2EG	$8.9 \times 10^{-11} \pm 0.8 \times 10^{-11}$	This work
313	1ChCl:2EG	$1.4 \times 10^{-10} \pm 0.1 \times 10^{-10}$	This work
323	1ChCl:2EG	$2.9 \times 10^{-10} \pm 0.5 \times 10^{-11}$	This work
343	1ChCl:2EG	$4.5 \times 10^{-10} \pm 0.3 \times 10^{-10}$	This work
373	1-methylimidazolium trifluoromethylsulfonate	7.7×10^{-9}	[34]
363	1ChCl:2U	7.8×10^{-9}	[35]
353	urea/1-ethyl-3-methylimidazolium	5.5×10^{-9}	[36]
313	1ChCl:2EG	7.1×10^{-10}	[37]
–	hybrid eutectic sulfolane/water	5.0×10^{-12}	[38]

in the electrolytes: 94% Zn and 6% Co from 0.4 mol L^{-1} $ZnCl_2$ + 0.025 mol L^{-1} $CoCl_2$; and 97% Co and 3% Zn from 0.025 mol L^{-1} $ZnCl_2$ + 0.4 mol L^{-1} $CoCl_2$. This shows that the use of 1ChCl:2EG allows excellent control of the desired chemical composition for Zn-Co deposits.

As for morphology, Fig. 2b illustrates the copper substrate surface after mechanical grinding and polishing processes, where only the inherent grooves of metal erosion are observed. The results also indicated that all electrodeposits ensured a complete surface coating, proving the efficiency of the electrochemical conditions employed. For Zn coating (Fig. 2c), individual crystallites are seen, while the Co coating (Fig. 2d) exhibits dendritic shapes. The same characteristics are seen when any one of these cations is present as a major part of the electrolyte. Regardless of the proportion tested for each cation, observing at a higher magnification, the Zn-Co coatings (Fig. 2e and f) showed cracked morphological patterns, which have a high surface area and are considered excellent catalysts for electrochemical reactions. Table 2 shows the concentration of precursors tested in each electrolytic bath, in addition to the percentage of Zn, Co and Zn-Co measured by EDS in each coating.

XRD analyses were conducted to evaluate the crystalline structure of Zn, Co, and Zn-Co films. Fig. 3 shows the diffraction patterns before and after modification of copper substrates in deep eutectic solvent. According to ICDD/JCPDS database, the XRD data obtained indicate characteristic peaks associated with Cu with a face-centered cubic structure (card 85-1326), hexagonal metallic forms of Zn (card 03-065-5973), Co (card 15-0806), $Zn_{96}Co_4$ and Zn_3Co_{97} alloys (card 23-1390), besides rhombohedral $Co_2(OH)_3Cl$ (space group R-3m #166). The presence of the coatings also denotes high quality of the modifications carried out on the electrode substrate (see also the surface plasmon resonance results, Fig. S4 in Supplementary Material). On the other hand, the presence of $Co_2(OH)_3Cl$ shows that when Co^{2+} is electro-immobilized individually, parallel equilibria can be formed, leading to the formation of soluble salts and loss of coating stability. Although the same trend has not been registered for Zn^{2+}, Zn-Co coatings tend to be

Table 2
Composition of metallic coatings estimated by energy dispersive X-ray spectroscopy.

Bath	Precursor concentration (mol L^{-1})		Coatings composition (%)		Sample label
	$ZnCl_2$	$CoCl_2$	Zn	Co	
I	0.4	–	100	0	Zn
II	0.4	0.025	96	4	$Zn_{96}Co_4$
III	0.025	0.4	3	97	Zn_3Co_{97}
IV	–	0.4	0	100	Co

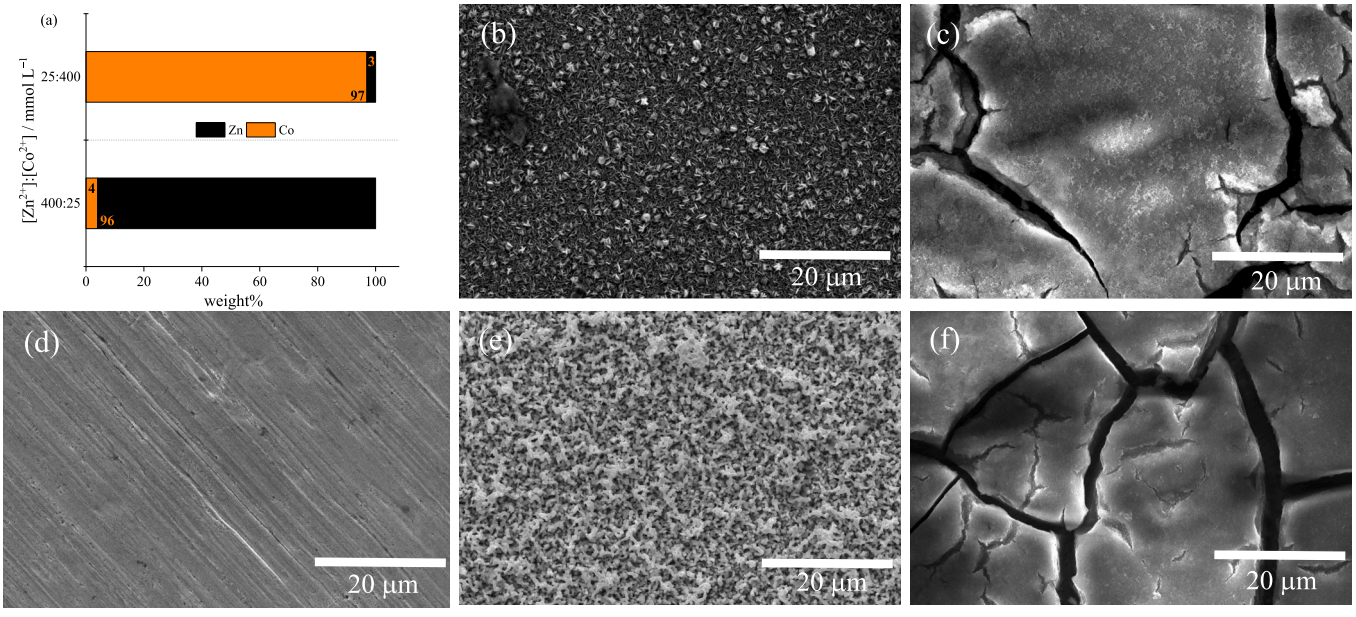

Fig. 2. (a) Metallic composition, along with the SEM images of (b) Cu substrate, (c) Cu/Zn, (d) Cu/Co, (e) $Cu/Zn_{96}Co_4$ and (f) Cu/Zn_3Co_{97}. The micrographs illustrated in b-d and e-f were recorded with 500- and 1000-times magnification, respectively.

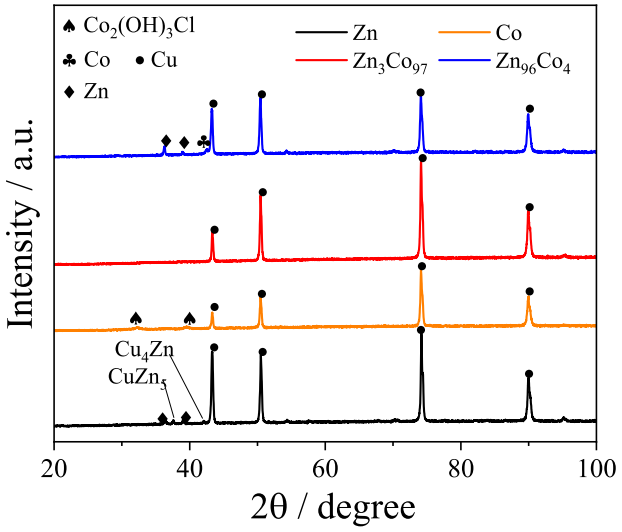

Fig. 3. XRD pattern of Zn, Co, and Zn-Co coatings, electrodeposited on Cu substrate.

more stable and suitable as electrocatalysts, as will be demonstrated later. No peaks resulting from impurities were detected, reaffirming the success in the electrosynthesis of the different metallic materials.

3.4. HER electrocatalysis

The overall performance of metallic substrates and coatings towards HER electrocatalysis is summarized in Fig. 4. The steady state curves obtained by LSV at 5 mV s^{-1} (Fig. 4a), using 1 mol/L KOH at 333 K as electrolyte, indicate the following onset potential order: Zn_3Co_{97} < $Zn_{96}Co_4$ < Co < Zn < Cu. This result proves that Zn-Co alloys are more promising as HER electrocatalysts, in addition to providing higher hydrogen production yields at lower potentials [46]. Even so, it is important to point out that all tested coatings performed better than the unmodified copper substrate, used as one of the standard electrode materials in studies with hydrogen production by water splitting.

Under alkaline conditions, the Tafel diagrams (Fig. 4b) are concentrated in a narrow overpotential range (≈ 150–320 mV dec^{-1}), suggesting that the HER mechanism for all the films is not affected by their thickness [47]. However, observing the Tafel fits, there are changes in slope values and, consequently, greater reaction rate on the Zn_3-Co_{97} coating (kinetic constant = 108.2 ± 0.74 mV dec^{-1}). About the surface stability, evaluated by potential variations at a current density of 10 mA cm^{-2} applied for 100 h of electrolysis (Fig. 4c), the greatest stability trend is seen for coatings that work at lower overpotentials (Co- and Zn_3Co_{97}-based coatings), possibly because they are less exposed to corrosion conditions and/or surface fouling by reaction by-products, which lead to variations in ohmic resistance. The electrochemical behavior demonstrated by the Cu substrate, Cu/Zn and Cu/$Zn_{96}Co_4$ is like that registered for AISI 304 stainless steel (overpotential variation from 100 mV to 300 mV during electrolysis), requiring higher potentials to promote HER and showing that the presence of cobalt contributes positively to catalyze this electrochemical reaction, including as an additive in metallic alloys. Zn_3Co_{97} coatings had the lowest overpotential variation among all the analyzed materials.

Values of electrochemical active surface area (ECSA) for catalysts were estimated from them electric double layer capacitance (C_{dl}). Cyclic voltammetric profiles of Zn, $Zn_{96}Co_4$, Zn_3Co_{97} and Co electrodes were recorded in a non-Faradic region (±0.05 V vs. reversible hydrogen electrode (RHE) in relation on E_{OCP} (t = 180 s)) at different scan rates (2.5, 5, 10 and 15 mV s^{-1}) in 1 mol/L KOH (Figs. S1 and S2 in the

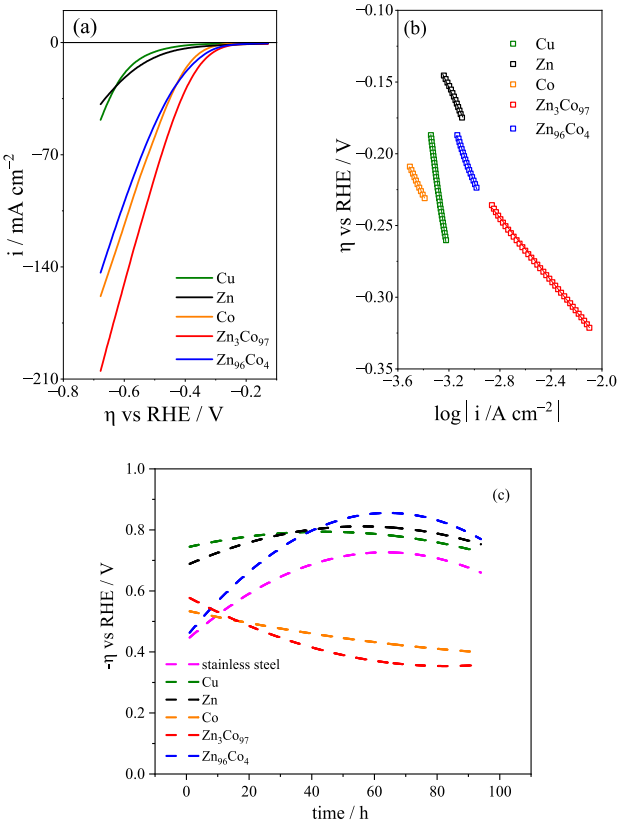

Fig. 4. (a) Polarization curves carried out with different catalysts at 0.5 mV s^{-1}. (b) The corresponding Tafel slopes. (c) Electrochemical stability tests of the catalysts, evaluated at 10 mA cm^{-2} and 333 K for 100 h. Supporting electrolyte: 1 mol L^{-1} KOH.

Supplementary Material). For comparison purposes, Table 3 presents Tafel coefficients (^{-}b), exchange current densities (i_0) and estimated overpotentials (|η|) for HER on each catalyst, obtained from fitting LSV data at 5 mV s^{-1} and using 1 mol L^{-1} KOH at 298.15 K. Now the values were normalized by geometric area and ECSA, as can be seen in Fig. S2 and Table S1 (in the Supplementary Material). These results corroborate the SEM images obtained in Fig. 3: the coating with the highest electroactive area ($Zn_{96}Co_4$) showed higher roughness, accompanied by Zn_3Co_{97}, which showed cracks.

As already stated earlier, the Cu substrate requires a highest |η| value (546 mV) to achieve a current density of 10 mA cm^{-2} during HER, followed by Zn (509 mV), Co (372 mV), $Zn_{96}Co_4$ (355 mV) and Zn_3Co_{97} (333 mV), reiterating the better electrocatalytic effect of the latter [48]. This sequence does not change even working at 10 times higher current densities. In addition, according to Banoth, Kandula and Kollu, it is desirable that an electrocatalytic material presents low values of Tafel slope accompanied by high values of exchange current [49]. When this occurs, high operating current densities can be achieved without a significant increase in overvoltage, which leads to lower operating costs [49]. Thus, the ^{-}b and i_0 values presented by the Zn_3Co_{97} and Co coatings are also indicative of their higher electrocatalytic activity compared to the others.

For Zn_3Co_{97}, comparing the Tafel parameters obtained in this study with previously published ones (Table 3), the values of ^{-}b and |η| were higher than those reported with Zn-Co-S, CoZn, NiCoZn e $Zn_{85}Ni$ coatings, but i_0 values were lower [46,48,50–52]. Since water molecules are precursors of HER by electrolysis, variations in the Tafel parameters may be due to uncompensated ohmic drop, so that small stoichiometric changes are sufficient to cause significant influences on the electrochemical reaction. Therefore, even more satisfactory results than those

Table 3
Electrochemical parameters obtained with different metallic coatings developed to produce hydrogen in 1 mol L^{-1} KOH at 298.15 K.

Catalyst	$-b$ mV dec^{-1}	i_0 A cm^{-2}	$i_{0\ ECSA}$ A cm^{-2}	$\|\eta\|$ (10 mA cm–2) mV	$\|\eta\|$ (100 mA cm–2) mV	Reference
Copper	622.2 ± 2.04	2.27 × 10^{-4} ± 1.80 × 10^{-5}	–	546	–	this work
Zn	233.1 ± 64.3	1.20 × 10^{-4} ± 2.86 × 10^{-5}	1.09 × 10^{-6} ± 2.60 × 10^{-7}	509	–	this work
$Zn_{96}Co_4$	247.6 ± 15.5	1.24 × 10^{-4} ± 5.33 × 10^{-5}	9.63 × 10^{-8} ± 5.42 × 10^{-8}	355	600	this work
Zn_3Co_{97}	108.2 ± 0.74	8.57 × 10^{-6} ± 3.28 × 10^{-7}	2.12 × 10^{-8} ± 8.12 × 10^{-10}	333	524	this work
Co	191.4 ± 3.20	2.52 × 10^{-5} ± 2.56 × 10^{-6}	8.42 × 10^{-8} ± 8.53 × 10^{-9}	372	578	this work
Zn-Co-S	86.3	–	–	176	–	[50]
CoZn	96	3.80 × 10^{-3}	–	–	240	[51]
NiCoZn	81	1.62 × 10^{-3}	–	–	140	[51]
$Zn_{85}Ni$	–	0.30 × 10^{-4}	–	95*	–	[46]

*not mentioned.

obtained in this work can be achieved from more detailed studies about the reaction mechanism and surface reactivity of the coatings.

4. Conclusions

Zn, Co, and Zn-Co alloys, produced electrochemically from 1ChCl:2EG DES, are functional materials to produce hydrogen in an alkaline medium, achieving remarkable electrocatalytic effect. The potentiostatic electrodeposition of these coatings allows a good stoichiometric control of the metallic constituents, and these materials achieved a better performance at higher temperatures, due to the reduction in electrolyte viscosity, charge-transfer resistance and increase in the diffusion coefficient of the precursor cations. Increasing Co content in coatings leads to morphological organization changes, resulting in cracked surfaces that have high surface area and directly contribute to HER electrocatalysis. Among the coatings studied, Zn_3Co_{97} was the one that showed the best performance in terms of ^{-}b, i_0 and $|\eta|$, therefore it is the most promising to produce hydrogen by water splitting.

CRediT authorship contribution statement

Deomar N. Rodrigues-Júnior: Investigation, Methodology, Writing – original draft, Formal analysis. **Natalia G. Sousa:** Investigation, Formal analysis. **F. Murilo T. Luna:** Resources. **Thiago M.B.F. Oliveira:** Writing – review & editing. **Dieric S. Abreu:** Investigation, Formal analysis, Writing – review & editing. **Walther Schwarzacher:** Writing – review & editing. **Pedro de Lima-Neto:** Resources. **Adriana N. Correia:** Conceptualization, Resources, Writing – review & editing, Supervision, Project administration, Funding acquisition.

Declaration of Competing Interest

The authors declare that they have no known competing financial interests or personal relationships that could have appeared to influence the work reported in this paper.

Acknowledgments

This study was financed in part by the Coordenação de Aperfeiçoamento de Pessoal de Nível Superior - Brasil (CAPES) – Finance Code 001. The authors thank the financial support given by the following Brazilian funding agencies: Coordenação de Aperfeiçoamento de Pessoal de Nível Superior (CAPES), Conselho Nacional de Desenvolvimento Científico e Tecnológico (CNPq) and Fundação Cearense de Apoio ao Desenvolvimento Científico e Tecnológica (FUNCAP). A.N. Correia gratefully acknowledges funding provided by CNPq (proc. 405596/2018-9 and 305136/2018-6). P. de Lima-Neto thanks the financial support received from CNPq (proc. 408626/2018-6 and 304152/2018-8). N. G. Sousa thanks CNPq for her grant (proc. 141171/2021-9). D. S. Abreu thanks FINEP (CV. 01.22.0174.00 BIONANO SPR) and CNPq (proc. 407954/2022-8) for financial support. The authors would like to thank the Central Analítica-UFC/CT-INFRA/MCTI-SISANO/Pró-Equipamentos CAPES for the support.

Appendix A. Supplementary data

Supplementary data to this article can be found online at https://doi.org/10.1016/j.jelechem.2023.117785.

References

[1] R. Shilpa, K.S. Sibi, S.R. Sarath Kumar, R.K. Pai, R.B. Rakhi, Electrocatalysts for hydrogen evolution reaction, in: Mater. Hydrog. Prod. Conversion, Storage, Wiley, 2023: p. 115-146. doi: 10.1002/9781119829584.ch5.
[2] C. Pi, Z. Zhao, X. Zhang, B. Gao, Y. Zheng, P.K. Chu, L. Yang, K. Huo, In situ construction of γ-MoC/VN heterostructured electrocatalysts with strong electron coupling for highly efficient hydrogen evolution reaction, Chem. Eng. J. 416 (2021), 129130, https://doi.org/10.1016/j.cej.2021.129130.
[3] C. Feng, B. Xin, H. Li, Z. Jia, X. Zhang, B. Geng, Agaric-like cobalt diselenide supported by carbon nanofiber as an efficient catalyst for hydrogen evolution reaction, J. Colloid Interface Sci. 610 (2022) 854–862, https://doi.org/10.1016/j.jcis.2021.11.130.
[4] X. Wang, R. Su, H. Aslan, J. Kibsgaard, S. Wendt, L. Meng, M. Dong, Y. Huang, F. Besenbacher, Tweaking the composition of NiMoZn alloy electrocatalyst for enhanced hydrogen evolution reaction performance, Nano Energy 12 (2015) 9–18, https://doi.org/10.1016/j.nanoen.2014.12.007.
[5] Z. Xu, Q. Zhu, X. Xi, M. Xing, J. Zhang, Z-scheme CdS/WO_3 on a carbon cloth enabling effective hydrogen evolution, Front. Energy 15 (2021) 678–686, https://doi.org/10.1007/s11708-021-0768-6.
[6] L. Chang, Z. Sun, Y.H. Hu, 1T phase transition metal dichalcogenides for hydrogen evolution reaction, Electrochem. Energy Rev. 4 (2021) 194–218, https://doi.org/10.1007/s41918-020-00087-y.
[7] H. Wu, C. Feng, L. Zhang, J. Zhang, D.P. Wilkinson, Non-noble metal electrocatalysts for the hydrogen evolution reaction in water electrolysis, Electrochem. Energy Rev. 4 (2021) 473–507, https://doi.org/10.1007/s41918-020-00086-z.
[8] M. Plevová, J. Hnát, K. Bouzek, Electrocatalysts for the oxygen evolution reaction in alkaline and neutral media. A comparative review, J. Power Sources 507 (2021), 230072, https://doi.org/10.1016/j.jpowsour.2021.230072.
[9] T. Lim, S.-K. Kim, Non-precious hydrogen evolution reaction catalysts: Stepping forward to practical polymer electrolyte membrane-based zero-gap water electrolyzers, Chem. Eng. J. 433 (2022), 133681, https://doi.org/10.1016/j.cej.2021.133681.
[10] M. Nemiwal, T.C. Zhang, D. Kumar, Graphene-based electrocatalysts: Hydrogen evolution reactions and overall water splitting, Int. J. Hydrog. Energy 46 (2021) 21401–21418, https://doi.org/10.1016/j.ijhydene.2021.04.008.
[11] V.D. Nithya, Recent advances in CoSe2 electrocatalysts for hydrogen evolution reaction, Int. J. Hydrog. Energy 46 (2021) 36080–36102, https://doi.org/10.1016/j.ijhydene.2021.08.157.
[12] S. Zhang, X. Zhang, Y. Rui, R. Wang, X. Li, Recent advances in non-precious metal electrocatalysts for pH-universal hydrogen evolution reaction, Green Energy Environ. 6 (2021) 458–478, https://doi.org/10.1016/j.gee.2020.10.013.
[13] A. Ali, F. Long, P.K. Shen, Innovative strategies for overall water splitting using nanostructured transition metal electrocatalysts, Electrochem. Energy Rev. 5 (2022) 1, https://doi.org/10.1007/s41918-022-00136-8.
[14] R. Zahra, E. Pervaiz, M. Yang, O. Rabi, Z. Saleem, M. Ali, S. Farrukh, A review on nickel cobalt sulphide and their hybrids: Earth abundant, pH stable electro-catalyst for hydrogen evolution reaction, Int. J. Hydrogen Energy 45 (2020) 24518–24543, https://doi.org/10.1016/j.ijhydene.2020.06.236.
[15] M. Ďurovič, J. Hnát, K. Bouzek, Electrocatalysts for the hydrogen evolution reaction in alkaline and neutral media. A comparative review, J. Power Sources 493 (2021), 229708, https://doi.org/10.1016/j.jpowsour.2021.229708.

[16] G. Gao, W. Wang, Y. Wang, Z. Fu, L. Liu, Y. Du, Z. Li, Y. Liu, L. Wang, Synergistic coupling of NiCoS nanorods with NiCo-LDH nanosheets towards highly efficient hydrogen evolution reaction in alkaline media, J. Electroanal. Chem. 943 (2023), 117622, https://doi.org/10.1016/j.jelechem.2023.117622.
[17] Z. Zhai, H. Li, C.-a. Zhou, H. Zheng, Y. Liu, W. Yan, J. Zhang, Anisotropic Strain Boosted Hydrogen Evolution Reaction Activity of F-NiCoMo LDH for Overall Water Splitting, J. Electrochem. Soc. 170 (3) (2023) 036509.
[18] C.L. Fan, D.L. Piron, H.J. Miao, M. Rojas, Hydrogen evolution in alkaline water on cobalt electrodeposits prepared from baths containing different anions, J. Appl. Electrochem. 23 (1993) 985–990, https://doi.org/10.1007/BF00266119.
[19] A. Maurya, S. Suman, A. Bhardwaj, L. Mohapatra, A.K. Kushwaha, Substrate dependent electrodeposition of Ni–Co alloy for efficient hydrogen evolution reaction, Electrocatalysis 14 (2023) 68–77, https://doi.org/10.1007/s12678-022-00773-z.
[20] V.S. Kublanovsky, Y.S. Yapontseva, Electrocatalytic properties of Co-Mo alloys electrodeposited from a citrate-pyrophosphate electrolyte, Electrocatalysis 5 (2014) 372–378, https://doi.org/10.1007/s12678-014-0197-y.
[21] T. Ling, T. Zhang, B. Ge, L. Han, L. Zheng, F. Lin, Z. Xu, W.-B. Hu, X.-W. Du, K. Davey, S.-Z. Qiao, Well-dispersed nickel- and zinc-tailored electronic structure of a transition metal oxide for highly active alkaline hydrogen evolution reaction, Adv. Mater. 31 (2019) 1807771, https://doi.org/10.1002/adma.201807771.
[22] C.K. Sumesh, Zinc oxide functionalized molybdenum disulfide heterostructures as efficient electrocatalysts for hydrogen evolution reaction, Int. J. Hydrog. Energy 45 (2020) 619–628, https://doi.org/10.1016/j.ijhydene.2019.10.235.
[23] Q. Cao, Z. Cheng, J. Dai, T. Sun, G. Li, L. Zhao, J. Yu, W. Zhou, J. Lin, Enhanced hydrogen evolution reaction over co nanoparticles embedded n-doped carbon nanotubes electrocatalyst with Zn as an accelerant, Small 18 (2022) 2204827, https://doi.org/10.1002/smll.202204827.
[24] S.S.V. Tatiparti, F. Ebrhimi, Potentiostatic versus galvanostatic electrodeposition of nanocrystalline Al–Mg alloy powders, J. Solid State Electrochem. 16 (2012) 1255–1261, https://doi.org/10.1007/s10008-011-1522-5.
[25] F. Endres, D. MacFarlane, and A. Abbott, Electrodeposition from ionic liquids, Electrodeposition from Ionic Liquids. p. 1-387, 2008, doi: 10.1002/9783527622917.
[26] K. Li, T. Ren, Z.Y. Yuan, T.J. Bandosz, Electrodeposited P-Co nanoparticles in deep eutectic solvents and their performance in water splitting, Int. J. Hydrog. Energy 43 (2018) 10448–10457, https://doi.org/10.1016/j.ijhydene.2018.04.136.
[27] C. Lei, H.F. Alesary, F. Khan, A.P. Abbott, K.S. Ryder, Gamma-phase Zn-Ni alloy deposition by pulse-electroplating from a modified deep eutectic solution, Surf. Coat. Technol. 403 (2020), 126434, https://doi.org/10.1016/j.surfcoat.2020.126434.
[28] A.P. Abbott, D. Boothby, G. Capper, D.L. Davies, R.K. Rasheed, Deep eutectic solvents formed between choline chloride and carboxylic acids: versatile alternatives to ionic liquids, J. Am. Chem. Soc. 126 (2004) 9142–9147, https://doi.org/10.1021/ja048266j.
[29] A. Srivastava, P. Sahu, M. S. Murali, Sk. M. Ali, M. Sahu, J. S. Pillai, and N. Rawat, New deep eutectic solvents based on imidazolium cation: Probing redox speciation of uranium oxides by electrochemical and theoretical simulations, J. Electroanal. Chem. vol. 901, p. 115752, 2021.
[30] A.S.C. Urcezino, L.P.M. Dos Santos, P.N.S. Casciano, A.N. Correia, P. De Lima-Neto, Electrodeposition study of Ni coatings on copper from choline chloride-based deep eutectic solvents, J. Braz. Chem. Soc. 28 (2017) 1193–1203, https://doi.org/10.21577/0103-5053.20160278.
[31] J.C. Pereira, L.P.M. Santos, A.A.C. Alcanfor, H.B. de Sant'Ana, F.X. Feitosa, O. S. Campos, A.N. Correia, P.N.S. Casciano, P. de Lima-Neto, Effects of electrodeposition parameters on corrosion resistance of ZnSn coatings on carbon steel obtained from eutectic mixture based on choline chloride and ethylene glycol, J. Alloy. Compd. 886 (2021), 161159, https://doi.org/10.1016/j.jallcom.2021.161159.
[32] J.C. Pereira, L.P.M. Santos, A.A.C. Alcanfor, O.S. Campos, P.N.S. Casciano, A. N. Correia, P. de Lima-Neto, Electrochemical corrosion evaluation of new Zn-Sn-In coatings electrodeposited in a eutectic mixture containing choline chloride and ethylene glycol, Electrochim. Acta 407 (2022), 139647, https://doi.org/10.1016/j.electacta.2021.139647.
[33] L.P.M. dos Santos, R.M. Freire, S. Michea, J.C. Denardin, D.B. Araújo, E.B. Barros, A.N. Correia, P. de Lima-Neto, and Pedro de Lima-Neto, Electrodeposition of 1-D tellurium nanostructure on gold surface from choline chloride-urea and choline chloride-ethylene glycol mixtures, J. Mol. Liq. 288 (2019) 111038.
[34] H.F. Alesary, S. Cihangir, A.D. Ballantyne, R.C. Harris, D.P. Weston, A.P. Abbott, K. S. Ryder, Influence of additives on the electrodeposition of zinc from a deep eutectic solvent, Electrochim. Acta 304 (2019) 118–130, https://doi.org/10.1016/j.electacta.2019.02.090.
[35] Q. Chu, J. Liang, J. Hao, Electrodeposition of zinc-cobalt alloys from choline chloride–urea ionic liquid, Electrochim. Acta 115 (2014) 499–503, https://doi.org/10.1016/j.electacta.2013.10.204.
[36] X. Fu, C. Zhan, R. Zhang, B. Wang, H. Sun, J. Sun, Effect of temperature on mechanism and kinetics of electrochemical nucleation of copper in ChCl–based deep eutectic solvents, J. Solid State Electrochem. 26 (2022) 2713–2722, https://doi.org/10.1007/s10008-022-05282-z.
[37] M.V. Tesakova, S.M. Kuzmin, V.I. Parfenyuk, Electrodeposition of films of individual 5,10,15,20-tetrakis(3-aminophenyl)porphyrin metal complexes and their composite for electrocatalytic oxygen reduction, Inorg. Chem. Commun. 135 (2022), 109106, https://doi.org/10.1016/j.inoche.2021.109106.
[38] T.D.V. Phuong, L.M. Quynh, N.N. Viet, L.V. Thong, N.T. Son, V.-H. Pham, P. D. Tam, V.H. Nguyen, T.L. Manh, Effect of temperature on the mechanisms and kinetics of cobalt electronucleation and growth onto glassy carbon electrode using reline deep eutectic solvent, J. Electroanal. Chem. 880 (2021), 114823, https://doi.org/10.1016/j.jelechem.2020.114823.
[39] G. Panzeri, A. Accogli, E. Gibertini, S. Varotto, C. Rinaldi, L. Nobili, L. Magagnin, Electrodeposition of cobalt thin films and nanowires from ethylene glycol-based solution, Electrochem. Commun. 103 (2019) 31–36, https://doi.org/10.1016/j.elecom.2019.04.012.
[40] M. Li, Y. Li, Electrodeposition of zinc from zinc oxide and zinc chloride in 1-methylimidazolium trifluoromethylsulfonate ionic liquid, Prot. Met. Phys. Chem. Surfaces 56 (2020) 180–188, https://doi.org/10.1134/S2070205120010141.
[41] H. Yang, R.G. Reddy, Electrochemical kinetics of reduction of zinc oxide to zinc using 2:1 urea/ChCl ionic liquid, Electrochim. Acta 178 (2015) 617–623, https://doi.org/10.1016/j.electacta.2015.08.050.
[42] W. He, L. Shen, Z. Shi, B. Gao, X. Hu, J. Xu, Z. Wang, Zinc electrodeposition from zinc oxide in the urea/1-ethyl-3-methylimidazolium chloride at 353 K, Electrochemistry 84 (2016) 872–877, https://doi.org/10.5796/electrochemistry.84.872.
[43] K. Wang, J. Phelps, R. Abdolvand, J. Carter, H.A. Hamedani, Zinc nanoparticles electrodeposited on TiO2 nanotube arrays using deep eutectic solvents for implantable electrochemical sensors, ACS Appl. Nano Mater. 6 (2023) 8238–8249, https://doi.org/10.1021/acsanm.3c00511.
[44] C. Li, R. Kingsbury, A.S. Thind, A. Shyamsunder, T.T. Fister, R.F. Klie, K.A. Persson, L.F. Nazar, Enabling selective zinc-ion intercalation by a eutectic electrolyte for practical anodeless zinc batteries, Nat. Commun. 14 (2023) 3067, https://doi.org/10.1038/s41467-023-38460-2.
[45] T.K. Dang, N. Van Toan, C.M. Hung, N. Van Duy, N.N. Viet, L.V. Thong, N.T. Son, N. Van Hieu, T.u. Le Manh, Investigation of zinc electronucleation and growth mechanisms onto platinum electrode from a deep eutectic solvent for gas sensing applications, J. Appl. Electrochem. 52 (2) (2022) 299–309.
[46] G. Sheela, Zinc–nickel alloy electrodeposits for water electrolysis, Int. J. Hydrog. Energy 27 (2002) 627–633, https://doi.org/10.1016/S0360-3199(01)00170-7.
[47] F. Bao, E. Kemppainen, I. Dorbandt, R. Bors, F. Xi, R. Schlatmann, R. van de Krol, S. Calnan, Understanding the hydrogen evolution reaction kinetics of electrodeposited nickel-molybdenum in acidic, near-neutral, and alkaline conditions, ChemElectroChem 8 (2021) 195–208, https://doi.org/10.1002/celc.202001436.
[48] H. Ren, L. Yu, L. Yang, Z.H. Huang, F. Kang, R. Lv, Efficient electrocatalytic overall water splitting and structural evolution of cobalt iron selenide by one-step electrodeposition, J. Energy Chem. 60 (2021) 194–201, https://doi.org/10.1016/j.jechem.2021.01.002.
[49] P. Banoth, C. Kandula, and P. Kollu, Introduction to electrocatalysis, In: Noble metal-free electrocatalysts: new trends in electrocatalysts for energy applications, vol. 2, ch. 1, p. 1-37, 2022, doi: 10.1021/bk-2022-1432.ch001.
[50] B. Zhang, G. Yang, C. Li, K. Huang, J. Wu, S. Hao, J. Feng, D. Peng, Y. Huang, Phase controllable fabrication of zinc cobalt sulfide hollow polyhedra as high-performance electrocatalysts for the hydrogen evolution reaction, Nanoscale 10 (2018) 1774–1778, https://doi.org/10.1039/C7NR08097B.
[51] A. Döner, R. Solmaz, G. Kardaş, Enhancement of hydrogen evolution at cobalt–zinc deposited graphite electrode in alkaline solution, Int. J. Hydrog. Energy 36 (2011) 7391–7397, https://doi.org/10.1016/j.ijhydene.2011.03.083.
[52] R. Solmaz, G. Kardaş, Fabrication and characterization of NiCoZn–M (M: Ag, Pd and Pt) electrocatalysts as cathode materials for electrochemical hydrogen production, Int. J. Hydrog. Energy 36 (2011) 12079–12087, https://doi.org/10.1016/j.ijhydene.2011.06.101.